Bergink et al., http://www.jcb.org/cgi/content/full/jcb.201107050/DC1

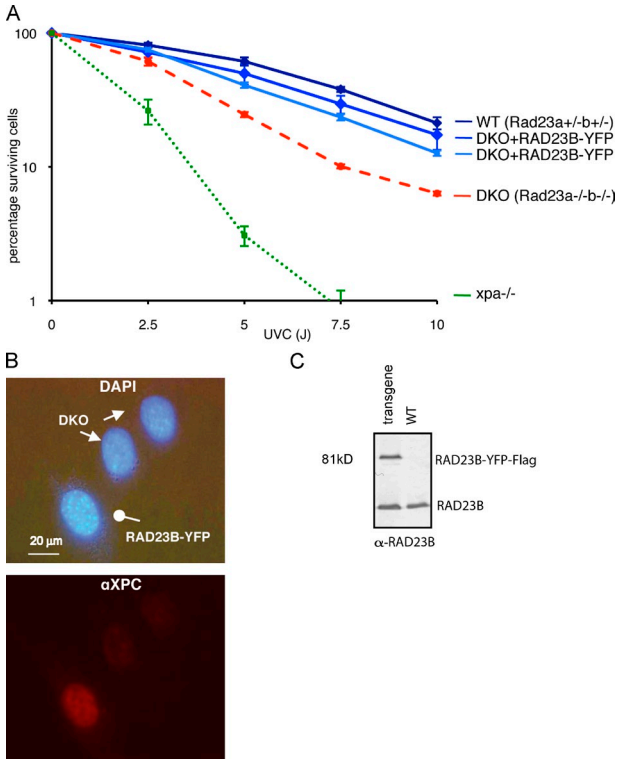

Figure S1. **RAD23B-YFP-FLAG is proficient in NER.** (A) UV colony survival assay of different MEFs, as indicated. Stable RAD23B-YFP-FLAG–expressing clones are not hypersensitive to UV light (similar to WT MEFs), whereas the parental Rad23a/b DKO is moderately UV sensitive compared with the high UV sensitivity of a control, complete NER-deficient $Xpa^{-/-}$ MEF. The y axis is in log scale. Survival assays were performed three times ($n = 3$). Error bars indicated SDs. (B) Comparative immunofluorescence analysis of XPC in DKO mixed with DKO cells that stably express RAD23B-YFP (identified by small beads in the cytoplasm; top). Endogenous XPC levels are increased in cells expressing RAD23B-YFP-FLAG in comparison with DKO cells (bottom). DKO cells are indicated with arrows, and DKO cells expressing mRAD23B-YFP are indicated by the blunt arrow. (C) Immunoblot analysis of whole-cell extracts from ES cells with or without two copies of the BAC RAD23B-YFP transgene. The blot is stained with anti-RAD23B (α-RAD23B) antibodies, and the migration of the fusion protein and endogenous protein is indicated.

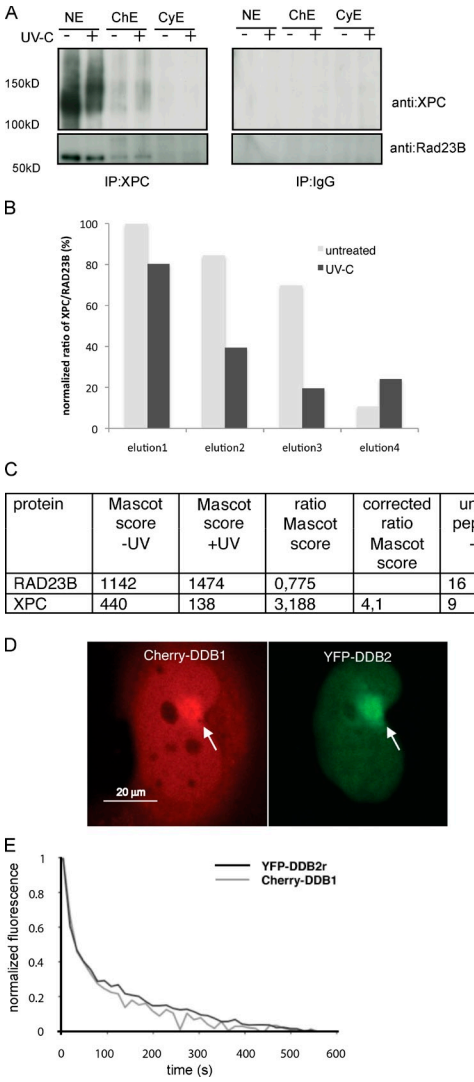

protein	Mascot score -UV	Mascot score +UV	ratio Mascot score	corrected ratio Mascot score	unique peptides -UV	unique peptides +UV
RAD23B	1142	1474	0,775		16	17
XPC	440	138	3,188	4,1	9	3

Figure S2. **XPC and RAD23B dissociate upon UV irradiation, whereas DDB1 and DDB2 remain a complex upon binding to damaged DNA.** (A) Immunoprecipitation (IP) of XPC from subcellular fractions soluble nuclear extract (NE), chromatin extract (ChE), and cytoskeletal extract (CyE), as indicated in Fig. 3 A. Less RAD23B coimmunoprecipitates with XPC after UV-C (20 J/m^2) treatment. Western blots of XPC and RAD23B are shown. Note that after UV, XPC migrates with different (slower) mobilities as compared with XPC isolated from non–UV-damaged cells, most likely a result of polyubiquitination. The loaded amount of precipitated material was adjusted to the total amount of XPC, including the slower migrating species. (B) Quantification of the immunoblot-derived signals as presented in Fig. 3 B. The blots were quantified using ImageGauge software (v4.23; Fujifilm). The ratios of XPC over RAD23B were obtained by dividing the XPC-derived signal with the RAD23B-derved signal after subtraction of the background for each. The different ratios are shown in the graph. (C) Semiquantitative mass spectrometry analysis of RAD23B-YFP-FLAG–XPC complexes isolated from ES cells containing two copies of the RAD23B-YFP-FLAG by immunoprecipitation on FLAG beads and subsequent elution by FLAG peptide. Complexes were isolated from ES cells 1 h after mock or UV treatment; the Mascot scores of RAD23B and XPC are shown. (D) Cells that express both Cherry-DDB1 and YFP-DDB2 were locally damaged with UV-C. Both Cherry-DDB1 and YFP-DDB2 accumulate on the local DNA damage. Arrows indicate the local damaged area. (E) Cells with a local damage containing both Cherry-DDB1 and YFP-DDB2 were subjected to iFRAP analyses, as in Fig. 3 E. DDB1 and DDB2 exhibit a similar dissociation rate from the local damage, indicative for a simultaneous dissociation of these proteins, which is in contrast to the differential dissociation of the RAD23–XPC complex.